Hydrol. Earth Syst. Sci. Discuss., 8, 4641–4699, 2011
www.hydrol-earth-syst-sci-discuss.net/8/4641/2011/
doi:10.5194/hessd-8-4641-2011

Hydrology and Earth System Sciences Discussions

A structure generator for modelling the initial sediment distribution of an artificial hydrologic catchment

T. Maurer[1], **A. Schneider**[1], **and H. H. Gerke**[2]

[1]Research Centre Landscape Development and Mining Landscapes, Brandenburg University of Technology, Cottbus, Germany
[2]Institute of Soil Landscape Research, Leibniz-Centre for Agricultural Landscape Research (ZALF), Muencheberg, Germany

Received: 15 April 2011 – Accepted: 27 April 2011 – Published: 9 May 2011

Correspondence to: T. Maurer (maurer@tu-cottbus.de)

Published by Copernicus Publications on behalf of the European Geosciences Union.

Abstract

Artificially-created hydrological catchments are characterized by sediment structures from technological construction processes that can potentially be important for modelling of flow and transport and for understanding initial soil and ecosystem development. The subsurface spatial structures of such catchments have not yet been sufficiently explored and described. Our objective was to develop a structure generator programme for modelling the 3-D spatial sediment distribution patterns depending on the technical earth-moving and deposition processes. For the development, the artificially-constructed hydrological catchment "Chicken Creek" located in Lower Lusatia, Germany, served as an example. The structure generator describes 3-D technological sediment distributions at two scales: (i) for a 2-D-vertical cross-section, texture and bulk density distributions are generated within individual spoil cones that result from mass dumping, particle segregation, and compaction and (ii) for the whole catchment area, the spoil cones are horizontally arranged along trajectories of mass dumping controlled by the belt stacker-machine relative to the catchment's clay layer topography. The generated 3-D texture and bulk density distributions are interpolated and visualized as a gridded 3-D-volume body using 3-D computer-aided design software. The generated subsurface sediment distribution for the Chicken Creek catchment was found to correspond to observed patterns although still without any calibration. Spatial aggregation and interpolation in the gridded volume body modified the generated distributions towards more uniform (unimodal) distributions and lower values of the standard deviations. After incorporating variations and pedotransfer approaches, generated sediment distributions can be used for deriving realizations of the 3-D hydraulic catchment structure.

HESSD

8, 4641–4699, 2011

1 Introduction

Hydrologic catchments can be defined as discrete geo-bodies of consolidated or unconsolidated rock with a given 3-D geometry. They are normally delineated at the bottom by a layer of rocks or sediments with low permeability that restricts water percolation, forming the subsurface catchment (Brutsaert, 2005). At the surface, the catchment is characterized by topography and land use conditions. Problems regarding hydrologic modelling are often related to uncertainties in subsurface structures and hydraulic properties and with respect to the spatial extent and geometry of the bottom and lateral boundaries. Also, discrepancies in lateral delineation between soil surface and bottom layer can occur. For better identification of catchment boundaries, hydrogeological data (i.e., spring discharge, soil and geological surveys, tracer tests, and isotopes) have been combined with modelling (e.g. Benischke et al., 2010), and digital elevation models (DEMs) have been used (Hammond and Han, 2006).

Moreover, the spatial distribution of hydraulic properties within a catchment depending on the distribution and properties of the solid phase was subject of recent experimental investigations and estimation efforts. Gascuel-Odoux et al. (2010), for example, tested the impact of spatial heterogeneity of hydraulic conductivity on the prediction quality of a hydrologic model (i.e., Hill-Vi). Similarly, Gauthier et al. (2009) tested effects of increasingly complex scenarios of spatial heterogeneity on model predictions. An evaluation of the applicability of pedotransfer functions for the spatial modelling of soil hydraulic properties (Stumpp et al., 2009) unanimously found that prediction quality increases when assuming complex spatial distributions of soil hydraulic properties; results stress the importance of verifying and conditioning spatial models with measured data.

The spatial structures (e.g., along layers or facies of fluvial deposits) in catchments depend on particular processes of catchment formation: for instance, alluvial processes produce sedimentary structures while the structure of aquifers in karst regions depends on the distribution of fractures (e.g., Siemers and Dreybrodt, 1998). Structural

HESSD
8, 4641–4699, 2011

differences between the alluvial and karstic domains of the Orleans valley aquifer were found to result in a "dynamically confined system" with reduced hydrochemical exchange between both domains (Le Borgne et al., 2005). Mozley and Davis (1996) showed that primary structures in alluvial aquifers induce the formation of secondary structures such as concretions. For an experimental catchment, the impact of structural heterogeneity on hydrology (e.g. soil moisture patterns) was quantified using the HydroGeoSphere programme (Sciuto and Diekkrueger, 2010). Soil structural and hydrological heterogeneity governs flow and transport processes, which ultimately affect soil development and biotic processes (e.g., Gutierrez-Jurado et al., 2006).

Recently, geophysical approaches are increasingly being used for the non-invasive exploration of subsurface structures (e.g., Hinschberger et al., 2006, Bosch and Muller, 2005). However, the integration of such methods into watershed modelling is not yet well established (Robinson et al., 2008). A classical approach in geosciences for the description of structural heterogeneity is to utilize geostatistical methods. The spatial interpolation between measurement points is generally not suited for depicting sharply bounded structures like different sediment facies (Michael et al., 2010). More sophisticated methods like multi-point geostatistical techniques excel indeed at respecting local data and allow more realistic representations of spatial patterns, but are still dependent on the input of training images that already purport the spatial heterogeneity (Hu and Chugunova, 2008).

Given the shortcomings of spatial modelling based on using "pure" geostatistics (Koltermann and Gorelick, 1996), alternative modelling approaches have been developed in recent years: Grunwald et al. (2000) implemented the Virtual Reality Modelling Language (VRML) in combination with soil data, topographical attributes, and kriging to create 3-D representations of soil landscapes; Zappa et al. (2006) conditioned 3-D geostatistical simulations using "model blocks" derived from soil profiles that represent facies associations to model a glacio-fluvial aquifer; Moreton et al. (2002) used a physical model of the subsurface depositional stratigraphy of a braided river system to feed object-based digital reservoir models; Sech et al. (2009) developed a surface-based

HESSD
8, 4641–4699, 2011

modelling approach that enables explicit representation of heterogeneity across a hierarchy of length scales.

Catchment and reservoir modelling approaches distinguish between object-based methods that distribute predefined "geobodies" within a model domain and process-based techniques that describe the physical processes rather than the existing structure (Michael et al., 2010). For instance, Gross and Small (1998) formulated a process model to simulate the development of river facies, and Miller et al. (2008) used a process-modelling approach to generate geologically realistic structures of turbidite fans. Their process-based spatial model was conditioned with measured data using geostatistical techniques (Michael et al., 2010). Such structure-generating methods produce only representations of the actual reservoir structures. Since the actual structures can never be reproduced adequately (de Marsily et al., 2005), consideration of uncertainties of the predicted spatial distributions is important.

Any process-based "structure generator" model that is able to reproduce the key structural elements requires basic knowledge of formation processes and of the arrangement of structural elements. Such information can most easily be gathered for artificial catchments, which have been comprehensively planned and constructed such that size, geometry, sediment composition, and boundaries are much better defined than natural systems. An artificial catchment thus qualifies as a large scale research tool for investigating hydrological problems and ecosystem development (cf., Hooper, 2001). Up to now, only a few of these open air laboratories were implemented: Gu and Freer (1995) describe experiments on three artificial experimental basins at the Chuzhou Hydrology Laboratory in Nanjing, China, ranging from 0.05 to 0.8 ha in size; Barbour et al. (2004) used mixtures of mineral material and peat placed over glacial mineral soil above a sealing saline-sodic shale surface for testing changes in hydraulic conductivities; and Nicolau (2002) investigated runoff generation and routing on artificial slopes derived from open cast mining reclamation. Depending on the size of the catchment construction, more or less "homogeneous" substrate distributions can be realized (Kendall et al., 2001).

HESSD
8, 4641–4699, 2011

Nevertheless, construction process-specific substrate heterogeneities may still have a considerable impact on hydrological processes. Knappe et al. (2004), for instance, found relatively high variability in seepage rates, which are probably reflecting the heterogeneity of forest-reclaimed overburden dumps in the central German lignite mining district. Tracer experiments by Hangen et al. (2005) on similar overburden spoil sediments in Lower Lusatia, Germany, indicated that flow processes are strongly influenced by structures such as inclined dumping structures and lignite fragments (cf. Gerke 2006)

For modelling such overburden spoil piles, the spatial heterogeneity of sediment texture and bulk density was considered by taking technical dumping and mixing processes into account (Buczko and Gerke, 2005a and b). When transferring these sediment structures into hydraulic and transport properties, the predicted flow paths reflected the internal structure of the artificial system.

The objective of this study was to develop a structure generator programme that models the 3-D spatial sediment distribution by considering the technical earth-moving and dumping processes and the geology and sediment composition at the outcrop site. The purposes of this process-based model were (i) to create a tool for the generation of 3-D-realizations of spatial sediment distributions in constructed catchments, (ii) to provide basic 3-D information for testing and comparing hydrological models (Hollaender et al., 2009) and for studying structure-and-process interdependencies, and (iii) to create 3-D catchments for simulating dynamic development of the initial condition.

In the following, we will first describe the modelling of the textural and density distribution in individual 2-D-vertical cross-sections (i.e., spoil cones) that result from the dumping of sediments. Then, these individual cones will be horizontally distributed in the catchment along trajectories following observed spoil ridges. Eventually, by combination and spatial interpolation, the distribution of the properties in the whole 3-D catchment volume will be constructed and the structure of the generated artificial catchment will be discussed.

HESSD
8, 4641–4699, 2011

2 Materials and methods

2.1 The artificial catchment "Chicken Creek"

The artificial hydrological catchment "Chicken Creek" (i.e., in German: "Hühnerwasser") is located in the post-mining recultivation area of the open cast lignite mine "Welzow Süd", about 20 km south of the city of Cottbus in the Lower Lusatian lignite mining area (Fig. 1). The 6-ha catchment was constructed by Vattenfall Europe Mining (VEM) to serve as headwaters for the restored streambed of the former "Chicken Creek". It has the form of a NW-SE running, almost rectangular, slightly inclined plane with a lengthwise extension of about 450 m and a transversal extension of about 160 m. The terrain inclines from NW to SE with an average of 3.5°. The size of the catchment is 5.9 ha at the soil surface and 6.1 ha at the bottom clay layer; thus the subsurface catchment is slightly larger than that at the surface. The catchment is draining in southeastern direction into a basin. The construction of the catchment was finished in October 2005. Since then, the soil-geosystem developed without human interference (Gerwin et al., 2009).

The climate in Lower Lusatia is temperate subcontinental, featuring a mean annual precipitation of 653 mm and an average temperature of 8.9 °C (Gerwin et al., 2009). In the summer months, thunderstorms accompanied by strong rainfalls are frequent. Those and other high intensity storms caused significant surface runoff and erosion on the initially initial surface and the rapid formation of a gully network during the first months of development in 2005/2006. Vegetation cover developed from pioneering plants (e.g. *Conyza Canadensis* followed by *Lotus corniculatus* and *Calamagrostis epigeios*) in 2006/2007 to a more diverse plant community in 2010, while patterns and density are explicitly governed by sediment heterogeneities; for instance, a significantly denser vegetation was observed on the more loamy part of the catchment (Zaplata et al., 2009).

The catchment was constructed using large-scale stacker technology. The material was excavated from the undisturbed excavation site of the open cast lignite mine and

HESSD
8, 4641–4699, 2011

was delivered over a distance of several kilometres by conveyor belts. The catchment foundation underneath was dumped by stackers above the conveyor bridge spoil (Fig. 2a) to form the base structure (Fig. 2b). Both conveyor bridge spoil and stacker base spoil consist predominantly of coarse-textured, tertiary overburden material. Above the base structure, a 1–3 m clay base liner of low permeability (Kendzia et al., 2008) was applied, acting as the catchment's aquiclude (Fig. 2c). It consists of the quaternary "Flaschenton" ("bottle clay"), which is fetched as a by-product of mining operations (Gerwin et al., 2011). The clay base liner forms an elongated, bowl-like subsurface structure, thus purporting groundwater flow towards the pond, respectively the single catchment outlet.

The uppermost covering layer consists of 1.5–3 m coarse-textured sandy overburden sediments of quaternary origin (Figs. 2d, e). These sandy-loamy sediments constitute the permeable catchment volume. The permeable sediment body is explicitly delimited to the sides by the clay base liner in the form of an elevated brim, which ends about 0.5–2 m below the ground surface (Fig. 2f). The resulting surface and subsurface catchments are widely, but not totally congruent. Due to technical reasons (i.e. the stepwise redeployment of stacker tracks), the construction was carried out strip-wise between May 2004 and October 2005, beginning with the easternmost strip 1, which was completed around August 2004 (Fig. 3a), and ending with the westernmost strip 4 in August/September 2005 (Fig. 3c). The time gap between the constructions of each strip resulted in the dumping of two slightly different materials on the eastern and western part of the uppermost layer (Fig. 3c). The stacker dumping technology produced characteristic structures, i.e. spoil ridges consisting of single overlapping spoil cones (Fig. 4a). This fragmentation in cones was caused by the rather stepwise sweep of the stacker arm. Between the eastern and western dumps remained a central trench (Fig. 3c). Between April and July 2005, this depression was filled by bulldozers, scraping material from both sides into the trench, thus producing significantly different internal structures in the centre of the catchment. After bulldozing, the catchment surface was flattened to remove any artificial unevenness (September/October 2005).

HESSD
8, 4641–4699, 2011

During the construction phase, spatial data were collected about the setting of the clay base liner. The main data source was the photogrammetric analysis of aerial photographs carried out by the mine-surveying department of Vattenfall Europe Mining (Table 1). These data covered mainly the area around the central trench and the southern area around the pond. A complete photogrammetric coverage of the clay base liner was not possible due to the limited number of aerial photographs taken during construction. Borehole field campaigns were carried out in the months after construction to collect data about the exact position of the base liner in areas which were not covered by the photogrammetric surveys. In order to define the subsurface catchment, several borehole campaigns were carried out to determine the borders of the base liner and, in particular, its peripheral topography (Gerwin et al., 2009; Maurer et al., 2009). Aerial photographs and corresponding DEMs from different points of time during construction ware also used to reconstruct the principal layout of construction elements and volumes (see Sect. 2.3).

Soil and sediment properties

The material used for construction of the covering layer consists of coarse-textured sediments (Table 2) in which the sand fractions (i.e., 2.0–0.063 mm particle diameter) dominate with an average of about 84 % (coarse sand 12.2 %, medium sand 45 %, fine sand 26.7 %), and with contents of about 9 % silt (i.e., 0.063–0.002 mm) and 7 % clay (i.e., <0.002 mm) only for the "fine earth" particles <2 mm). The pleistocene, mainly glacigenic material (Table 3) has relatively high skeleton (i.e., >2 mm) contents of about 12 % in relation to total mass. Due to the aforementioned separate delivery of two materials for the western and eastern part of the catchment, the average texture of each side shows noticeable differences: the eastern part has a 4 % higher sand content , and accordingly lower silt (3 % less) and clay (2 % less) contents than the western part (Table 2). The clay fraction is dominated by illite (41–60 %) and mixed-layer clay minerals (12–38 %; <50 % illite). Kaolinite (9–16 %) and vermiculite (3–4 %)

HESSD
8, 4641–4699, 2011

were found in relatively small amounts. More soil properties can be found in Gerwin et al. (2009).

Soil samples were taken between October 2005 and April 2006 in depths of 0–0.3 m and 0.3–1.0 m along a 20 × 20 m grid. Additional soil samples were taken in a 40 × 40 m grid in depths of 0–0.5, 0.5–1.0, 1.0–1.5 and 1.5–2.0 m. During the construction phase in January 2005, additional samples were taken from 11 spoil cones in approximately 0.5 m height above the clay base liner (Gerwin et al., 2009). These samples were used for X-ray diffraction analysis (Whittig and Allardice, 1986). Soil texture was determined after elimination of carbonates (H_2O_2 treatment was omitted because organic matter was absent) using wet sieving and the pipette method (Gee and Bauder, 1986).

Parent material of the outcrop at the excavation site

The parent material of the Chicken Creek sediment body was digged off by bucket excavators located in the forefront of the Welzow Süd mining area and delivered to the stacker via conveyor belts. Geological cross-sections (Fig. 4) depict the spatial configuration of quaternary and tertiary sediments along the excavator route in the year of construction (2004). Texture data are available for most of the geological units, albeit data about mineralogy is generally missing and were estimated from literature (e.g. Niemann-Delius et al., 2008; Piotrowski et al., 1999). Aerial photographs show that the Chicken Creek sediments were delivered in two separated batches in September and October 2004, for the eastern and western parts. The exact location of the excavator was not recorded for these dates, such that the selection of sediment type and geological unit became part of the generator model.

2.2 The structure generator model

The conceptual model considers the processes of parent material dumping and levelling of the catchment surface (Fig. 5). The generator considers two scales: 2-D

HESSD
8, 4641–4699, 2011

overburden spoil cones and catchment scale. First, the base material composition is defined considering the geologic conditions at the excavation site and mixing due to conveyor belt transport (Fig. 5a). Then, 2-D spoil cone cross-sections are constructed considering particle segregation at the cone flanks and compaction in the central zone. The geometric configuration of each individual spoil cone is considered as well, namely the distance to neighbouring spoil ridges (Fig. 5b). These structural elements are then aligned according to their known 3-D spatial configuration along the identified stacker trajectories (Fig. 5c). In a final step, data are aggregated and interpolated an a 3-D representation of the catchment using the GOCAD software (version 2009.3 patch 1, Paradigm Ltd., George Town, KY; Fig. 5d). The programme was written in Visual Basic for Applications (VBA, Microsoft Corp., Redmond) to ensure a straightforward incorporation of input data stored in Excel-spreadsheets.

Geometry of individual 2-D spoil cone cross sections

In the model, each spoil cone is virtually represented as a 2-D cross section consisting of gridded data points. The principal shape and the properties stored in the grid are basically governed by input parameters. Input parameters are directly derived from the recorded spatial settings or can have adjustable values. 2-D-cross sections of spoil cones are arranged in sequences with an adjustable horizontal spacing along the digitized spoil ridges. Spoil ridges are digitized as curve objects consisting of segments and nodes in GOCAD. Each node represents the position of a spoil cone cross section. By varying the density of nodes on the spoil ridge curve object in GOCAD, the horizontal distances between cross sections can be adjusted. Node coordinates are exported as ASCII files to serve as input data for the structure generator. The programme works off every 2-D cross section in the ASCII listing successively by considering the predefined spatial framework (i.e. slope angle, spoil cone height, oblique central axis, spacing between adjacent ridges, spatial orientation of the current ridge) in the outermost loop (Fig. 6).

HESSD
8, 4641–4699, 2011

From the pre-defined layer thickness $\underline{ds}_m$ (Table 4), the horizontal and vertical lengths of a layer m, dx_m and dz_m are calculated:

$$dx_m = \frac{ds_m}{\sin\alpha} \tag{1}$$

$$dz_m = \frac{ds_m}{\cos\alpha} \tag{2}$$

Using the pre-defined values for slope angle α, spoil cone height H and back width R (Table 4), the spoil cone length L can be calculated as:

$$L = \frac{2 \cdot H}{\tan\alpha} - \frac{H - (0.5 \cdot R \cdot \tan\alpha)}{\tan\alpha} \tag{3}$$

The initial impact point is defined as the point where the dumped material of a new spoil cone initially hits the surface. In most cases, depending on spoil cone position on the ridge and its height, this point is located on the flank of a neighbouring spoil ridge. The z-coordinate *Zinit* of the initial impact point is calculated first as:

$$Zinit = H - \left(\frac{\tan\alpha \cdot R}{1 + \tan\alpha \cdot \tan\beta} \right) \tag{4}$$

with β being the angle of the oblique central axis of the spoil cone cross section. The x-coordinate *Xinit* can then be defined as:

$$Xinit = R + \frac{Zinit}{\tan\alpha} \tag{5}$$

The total number of layers l within each spoil cone is calculated as:

$$l = \frac{Xinit - \frac{Zinit}{\tan\alpha}}{dx_m} \tag{6}$$

The example in Fig. 5b has eight layers ($l = 8$).

HESSD
8, 4641–4699, 2011

Spatial alignment of cone cross sections in the catchment

Raster points in cross sections need to be assigned to geographic coordinates and aligned correctly on the spoil ridge (Fig. 7). Since the routine handling the construction of the cross section grid uses internal coordinates, the correct geographic coordinates have to be calculated for each grid point separately at the beginning of each cycle. The correct spatial alignment can be derived from the vector $\overrightarrow{XY}_{\text{diff}}$ (height values are of no importance in this case) pointing from the current position pos1 towards the next cross section's position pos2:

$$\overrightarrow{XY}_{\text{diff}} = \begin{bmatrix} X_{\text{pos1}} \\ Y_{\text{pos1}} \end{bmatrix} - \begin{bmatrix} X_{\text{pos2}} \\ Y_{\text{pos2}} \end{bmatrix} = \begin{bmatrix} \text{Xdiff} \\ \text{Ydiff} \end{bmatrix} \tag{7}$$

Cross sections through spoil cones / spoil ridges thus have to be aligned perpendicular to $\overrightarrow{XY}_{\text{diff}}$. Vector transformation via vector rotation around the z-axis using a rotation angle λ determines the alignment vector $\overrightarrow{XY}_{\text{trans}}$.

The principle for a vector rotation around the z-axis is given in the rotation matrix **R**, and in Eq. (8):

$$\mathbf{R} = \begin{bmatrix} \cos\lambda & -\sin\lambda & 0 \\ \sin\lambda & \cos\lambda & 0 \\ 0 & 0 & 1 \end{bmatrix} \tag{8}$$

Thus, $\overrightarrow{XY}_{\text{trans}}$ can be calculated using:

$$\overrightarrow{XY}_{\text{trans}} = \begin{bmatrix} Xdiff \\ Ydiff \end{bmatrix} \cdot \cos 90° + \begin{bmatrix} -Ydiff \\ Xdiff \end{bmatrix} \cdot \sin 90° = \begin{bmatrix} Xtrans \\ Ytrans \end{bmatrix} \tag{9}$$

A distance unit *du* for the new alignment is calculated from the *Xtrans* and *Ytrans* components using Pythagoras' theorem:

$$du = \sqrt{\frac{L^2}{Xtrans^2 + Ytrans^2}} \tag{10}$$

HESSD
8, 4641–4699, 2011

Step lengths in the actual geographic coordinate system (WGS84) for the longitude (*Xstep*) and likewise for the latitude (*Xstep*) are then calculated:

$$Xstep = Xtrans \cdot \sqrt{\frac{(Xtrans \cdot du)^2}{L}} \tag{11}$$

$$Ystep = Ytrans \cdot \sqrt{\frac{(Ytrans \cdot du)^2}{L}} \tag{12}$$

The relative coordinates used to establish the 2-D-cross section are ultimately transferred into geographical coordinates using the calculated step lengths, here given for the transformation of the value for the longitude, *Xcoord*. Since cross sections are established using 1 cm steps, coordinates (in units of metres) are transformed in cm using:

$$Xcoord = Xorig - \frac{Xstep \cdot Xinit}{100} + \frac{Xcorel \cdot Xstep}{100} \tag{13}$$

With *Xorig* being the original position on the spoil ridge determined from dumping trajectories. Trajectories were derived by projecting aerial photos of spoil ridges onto the clay base liner surface DTM (Fig. 10a, Maurer et al., 2009).

Depending on their position on a ridge, cross sections are not properly aligned towards the stacker's position. This is a consequence of vector rotation. For example, for the east side of Chicken Creek catchment, stacker positions can be either "southeast" or "northeast" relative to spoil ridges. Whether the stacker was located in the NE or SE of the catchment can not be reconstructed. Assuming a relative stacker position in the southeast, cross sections located on ridges with a "northward" component need to be mirrored or flipped, otherwise they would point in the opposite direction as the "correctly" aligned cross sections. Before flipping, the initial impact point *Xinit* is subtracted

HESSD
8, 4641–4699, 2011

from the spoil cone length L (here given for the longitude respectively the geographical x-coordinate):

$$Xcoord = Xorig - \frac{Xstep \cdot (L\text{-}Xinit)}{100} + \frac{Xcorel \cdot Xstep}{100} \quad (14)$$

where *Xcorel* is the relative coordinate, i.e. the 1 cm increment in the outer for/next loop.

Flipping is realized in a separate routine after terminating the construction of a spoil cone cross section and the calculations for segregation and compaction. In principle, the routine exchanges coordinates of rows 1 to n, flipping columns 1 to m. In principle, the routine exchanges coordinates of opposite sides of rows 1 to n, flipping columns 1 to m according to the following matrix (also see Fig. 8):

$$\begin{bmatrix} x_{1,1}, y_{1,1}, z_{1,1} & \leftrightarrow & x_{1,m}, y_{1,m}, z_{1,m} \\ x_{1,2}, y_{1,2}, z_{1,2} & \leftrightarrow & x_{1,m-1}, y_{1,m-1}, z_{1,m-1} \\ \vdots & & \vdots \\ x_{1,\frac{m}{2}-1}, y_{1,\frac{m}{2}-1}, z_{1,\frac{m}{2}-1} & \leftrightarrow & x_{1,\frac{m}{2}+1}, y_{1,\frac{m}{2}+1}, z_{1,\frac{m}{2}+1} \\ \vdots & & \vdots \\ x_{n,\frac{m}{2}-1}, y_{n,\frac{m}{2}-1}, z_{n,\frac{m}{2}-1} & \leftrightarrow & x_{n,\frac{m}{2}+1}, y_{n,\frac{m}{2}+1}, z_{n,\frac{m}{2}+1} \end{bmatrix}$$

Definition of internal structure

Spoil cone cross sections are generated using two loops, the outer loop for the spoil cone lengths and the inner loop for the spoil cone height. This means that cross sections are assembled column-wise from left to right. This generates a 2-D grid where, in principle, each grid point is tested (a) whether it is inside or outside of the spoil cones, (b) whether it is on the left or right side of the central compaction zone and (c) to which layer m it will ultimately be assigned.

HESSD
8, 4641–4699, 2011

A grid point is located inside the spoil cone if the following conditions are true:

$$Zcorel < \tan\alpha \cdot Xcorel \tag{15}$$

$$Zcorel > \tan\alpha \cdot (Xcorel\text{-}R) \tag{16}$$

$$Xcorel\text{-}m + \frac{R}{2} < \frac{H\text{-}Zcorel}{\tan\alpha} \tag{17}$$

with *Zcorel* and *Xcorel* being the relative coordinates used during grid construction. The back width R is required to calculate where the spoil cone is "cut off" by the preceding spoil cone/spoil ridge.

In our model, we assume that the more or less oblique impact of sediment dumped by a stacker also causes spoil cone growth along an oblique central axis pre-defined as the oblique axis angle β (Table 4). As a consequence, layer thicknesses differ for the right and left sides of this axis. Thus, in a next step, the programme checks if grid points are located to the left or to the right of the oblique central axis of the spoil cone (left side check – condition is true if):

$$Xcorel - \frac{H}{\tan\alpha} > \frac{H\text{-}Zcorel}{\tan(90-\beta)} \tag{18}$$

In case that the angle of the central axis, β is oblique (i.e. not equal to 0°), two separate solutions for the assignment of grid cells to a layer need to be applied. In case the grid point is located to the left of the oblique central axis (Eq. 18 is true) then the grid point is assigned to layer m_i if two conditions are true:

$$Zcorel > \tan\alpha \cdot (Xcorel - (R+1) + (i-1) \cdot dx_m) \tag{19}$$

$$Zcorel < \tan\alpha \cdot (R+1) + i \cdot dx_m \tag{20}$$

In case the grid point is located to the right of the oblique central axis, the two following conditions are checked:

$$H\text{-}Zcorel > \tan\alpha \cdot \frac{Xcorel\text{-}H}{\tan\alpha} + (i-1) \cdot dxr_m \tag{21}$$

HESSD
8, 4641–4699, 2011

$$H\text{-}Zcorel > \tan\alpha \cdot \frac{Xcorel\text{-}H}{\tan\alpha} + i \cdot dxr_m \quad (22)$$

where dxr_m is being defined as the extension of layer m in x-direction for layers to the right of the central axis (Fig. 5b) according to:

$$dxr_m = \tan\alpha \cdot \left(\frac{\frac{Zd}{\tan\alpha} - Zd \cdot \tan\beta}{i} \right) \quad (23)$$

and with Zd being the distance $H - Zinit$, calculated using the formula:

$$Zd = \frac{\tan\alpha \cdot R}{1 + \tan\alpha \cdot \tan\beta} \quad (24)$$

Texture definition

In a first approach, we aim at reproducing spatial patterns of substrate heterogeneity as being observed in the post-mining area of Welzow-Süd. Here, substrate properties on a spoil ridge change significantly after a distance of about 10–30 m. In our model, we therefore define a "basic substrate" P for a series of 2-D cross sections (i.e. spoil cones). The according number of cross sections is randomly chosen between 3 and 9. Two randomly chosen sediment types $P1$ and $P2$ (Table 3) are mixed according to a random ratio *rnd*. Each of n particle size classes (here: skeleton, coarse, medium, fine sand and silt, clay), subscript i, in the basic substrate P_i is defined by mixing $P1_i$ and $P2_i$ using the random factor *rnd*, which lies between 0 and 1:

$$P_i = P1_i \cdot rnd + P2_i \cdot (1 - rnd) \quad (25)$$

It was assumed that each spoil cone has a slightly different composition *Psc* that differs from the basic substrate composition P. Variations are, however, supposed to occur in a relatively narrow limit with the maximum value *Csc*max, which is an adjustable

HESSD
8, 4641–4699, 2011

parameter (e.g. $Csc\max = 0.2$ allows fluctuations of maximal 20 %, Table 4). Particle distributions are varied at 2 scales:

(a) For the spoil cone, every spoil cone particle size class Psc_i^* is defined using:

$$Psc_i^* = P_i \cdot ((1 - Csc\max) + (rnd \cdot 2 \cdot Csc\max)) \quad (26)$$

After variation, the particle sum is uneven, so each of n particle fractions Psc_i^* has to be corrected to add up properly by using:

$$Psc_i = Psc_i^* / \sum_{i=1}^{n} Psc_i^* \quad (27)$$

(b) For each layer l, the particle distribution is further varied. We assume that each spoil cone shows slight heterogeneities in the internal substrate composition. The basic unit with an initially (i.e. before the dumping process) homogeneous substrate composition is defined as a "layer". We assume that layers are generated when a surge of the parent material flows down the spoil cone flanks, undergoing segregation processes at the same time. Layer thickness was defined ex ante. The initial substrate composition of each layer is varied in narrower limits as for spoil cone substrate variations using the pre-defined parameter $Csc l\max$ (Table 4):

$$Psc l_i = Psc_i \cdot ((1 - Csc l\max) + (rnd \cdot 2 \cdot Csc l\max)) \quad (28)$$

The random mixing of the often heterogeneous parent material and the application of the mixtures according to observed distances along a spoil ridge is designed to reproduce the specific patterns of stacker dumping. At this stage, the approach does not yet consider the geological configuration at the excavation site.

Segregation, compaction and bulk density distribution in individual cones

Following the establishment of one spoil cone cross section, the grid is filled layer-wise with the predefined substrate for each layer. In the model conception, the particle

HESSD
8, 4641–4699, 2011

distribution of the material is altered by segregation processes due to gravitational deposition, ultimately resulting in inverse grading. For the calculation of particle segregation, we adopted the empirical approach (Leibiger, 1964) that was based on observations and further developed by Buczko et al. (2001):

$$Pscl_i(x,z) = Pscl_{i,0} + \left(\frac{H_{\max}}{2} - H_k\right) \cdot \zeta_i \cdot Pscl_{i,0} \quad (29)$$

Here, $Pscl_i$(x,z) is the mass of the particle class i at the location with the coordinates (x,z) after segregation, $H_{\max}$, defined as the vertical distance from the reference elevation level H_k, is calculated as follows:

$$H_{\max} = Zinit + m \cdot dz_m \quad (30)$$

where dz_m is the vertical extension of the current layer m. The reference elevation level H_k is defined as the actual relative height coordinate *Zcorel*. ζi is an empirical dimensionless segregation factor gained from quaternary sediments in Lower Lusatia (Schlabendorf-Nord), ranging from −0.12 for clay particles to 0.12 for coarse sand particles and skeleton (Buczko et al., 2001).

2-D distribution of spoil bulk densities ρ_b are calculated based on the pre-defined dumping height and the calculated particle size distribution from Eq. (29) as:

$$\rho_b = w_U \cdot \left(\rho_{b0} + a \cdot \left(1 - \frac{U_m}{U}\right)\right) + w_R \cdot (\rho_{b0} + b \cdot (Z^* - 0.5)) \quad (31)$$

where ρ_{b0} is the initial estimated value (based on calibration data from spoil cone sampling) of the bulk density, w_U and w_R are weighing factors to account for the relative influences of the degree of non-uniformity and the random component on bulk density, U_m is the average value and U(x,z) is the value of the degree of non-uniformity at position (x,z). Z^* is a spatially uncorrelated random number between 0 and 1, while a and b are empirical factors accounting for the variation of the bulk density introduced by the grain size distribution and the random component (Buczko et al., 2001).

HESSD
8, 4641–4699, 2011

According to data from spoil cone sampling, we assume values of $\rho_{b0} = 1.2\,\mathrm{g\,cm^{-3}}$ for the whole spoil cone except for the central compaction area, where bulk density is calculated as a function of the changing dumping height and an elevated base value (here: $1.4\,\mathrm{g\,cm^{-3}}$) according to a linear regression equation (Matschak, 1969):

$$\rho_{b,c} = 1.4 + 0.0093 \cdot H_{\mathrm{D}} \tag{32}$$

where $\rho_{b,c}$ is the bulk density in the compaction zone in $\mathrm{g\,cm^{-3}}$ and H_{D} is the predefined sediment drop height in metre (Table 4).

The width of the central compaction zone was defined as the input parameter *Czone* (Table 4). Grid points are checked if they are located inside the central compaction zone using conditional inquiries:

$$Xcorel - \frac{Czone}{2} - \frac{H}{\tan\alpha} < \frac{H\text{-}Zcorel}{\tan(90-\beta)} \tag{33}$$

$$Xcorel + \frac{Czone}{2} - \frac{H}{\tan\alpha} > \frac{H\text{-}Zcorel}{\tan(90-\beta)} \tag{34}$$

If the condition is true, $\rho_{b0} = \rho_{b,c}$, otherwise $\rho_{b0} = 1.2$.

Data aggregation and output

Datasets generated for hundreds of spoil cone cross sections with generic original resolutions of $1\,\mathrm{cm^2}$ are far too voluminous to be handled properly with the currently available computing capabilities. Thus, prior to exportation to GOCAD, datasets need usually to be aggregated. Grid data of a spoil cone cross section are aggregated after the high resolution 2-D cross grid is established and correctly aligned and texture and bulk densities have been calculated. The degree of aggregation D_{A} is chosen ex ante (Table 4). D_{A} always aggregates the values stored in D_{A}^2 grid cells. For example, $D_{\mathrm{A}} = 3$ aggregates values contained in a 3×3 grid cell cluster. Along the spoil cone "slopes",

HESSD
8, 4641–4699, 2011

the aggregation routine checks whether the majority of cells in cluster lies inside the spoil cone. If the condition is true, the values in the cluster are aggregated, otherwise the cluster is filled with a nodata-value.

Aggregated data are then added to the opened ASCII save file. The save file contains for each aggregated grid point geographical coordinates (WGS 84), the height above sea level, skeleton content, coarse, medium and fine sand contents, silt content, clay content and bulk density values.

2.3 3-D volume model and interpolation

Determination of delineating surfaces and construction of a volume body

Based on the available photogrammetric and borehole data, a DEM of the clay base liner surface was constructed (Maurer et al., 2009). From the gridded surface, the subsurface catchment area was derived by applying the Deterministic 8 algorithm (O'Gallaghan and Mark, 1984). The subsurface catchment constitutes the lower delineating surface of the catchment's relevant sediment body.

For the construction of the upper delineating surface, a DEM dated 24 November 2005 was available. This dataset is the earliest recording of the initial soil surface, about 2 months after completion of the Chicken Creek catchment. The DEM was recorded during a routine photogrammetric survey by VEM. All vertical values in VEM photogrammetric datasets have an inherent error of +/−0.15 m associated with the given airplane altitude and camera configuration. Due to the obvious inconsistency of photogrammetric data and the spatially differentiated error in height values, the DEM was enhanced (cf. Schneider et al., 2009 and 2011).

From the delineating surfaces, a gridded volume body (Stratigraphic Grid or SGrid in GOCAD) was constructed in several steps (Schneider et al., 2011). The outlines of the two surfaces do not exactly coincide. The lateral boundary of the catchment was created from the borderlines of the two elevation models and split into parts inclined inward or outward. These surface parts were then used to define the model's lateral

HESSD
8, 4641–4699, 2011

boundary by "eroding" grid cells from the top and the bottom of the originally block-shaped volume body. The outline of the pond in November 2005 was digitized by visual interpretation of the model and the pond area was separated from the model (Schneider et al., 2011).

Spatial configuration of spoil ridges, volumes and masses

The spatial distribution of spoil ridges was derived by combining spectral information from aerial photographs with the spatial information contained in DEMs from the construction phase. Both aspects can be viewed simultaneously by overlying the DEMs with aerial photographs. Spoil ridges were manually digitized (Fig. 10a). Coverage of spoil ridges was incomplete due to the subsequent bulldozing of large areas. Aerial photographs from later stages trace spoil ridges locally, e.g. by discolouring of bare soil surfaces (probably as a consequence of different topsoil water contents) or vegetation patterns, which allowed a partial "interpolation" of the respective spoil ridges.

Horizontal distances between spoil ridges were derived by constructing surfaces from spoil ridge curve objects and measuring vertical distances after rotation in the vertical. For the segmentation of individual ridges, horizontal distances between spoil ridges crests were calculated as vertical distances between surface objects. This way, distance values get assigned to the points/nodes of the spoil ridge curve. This property value was then exported into an ASCII-file.

For the determination of the deposited and relocated sediment volumes, differential analysis of relevant DEMs was carried out. Applicable DEMs are for one that of the clay layer surface (*s_clay*) and the initial soil surface of November 2005 (*s_0511*). Furthermore, the DEM recorded at 19 October 2004 (*s_0410*) depicts the point of time during construction when the complete mass of the substrate has been applied on both halves of the catchment, but have not yet been bulldozed in a noteworthy degree (Fig. 10a). Thus, the differential volume $\{s\_0511 - s\_clay\}$ is that of the catchment's sediment body in its initial state after construction, $\{s\_0410 - s\_clay\}$ gives the spatial distribution (east

HESSD
8, 4641–4699, 2011

and west) of the originally applied sediment masses, and $\{s\_0410 - s\_0511\}$ gives the volumes abraded by subsequent bulldozing as well as the volume of the central trench that was filled up from both sides by bulldozing (Fig. 10b, c and Table 5). The two latter difference volumes give also information about (a) the presumed average height of spoil ridges (large areas were already bulldozed to a certain degree, so true ridge heights remain somehow speculative) and (b) to what extend these spoil ridges have been eventually "cut" by the final bulldozing process.

Spatial interpolation of structure generator data in GOCAD

After importing the ASCII data in GOCAD (here defined as "PointsSets", Fig. 11), the individual values were associated with the prepared 3-D volume body of the artificial catchment. This resulted in further aggregation of the data. Values were aggregated by calculating the arithmetic mean of all individual values contained in single cells.

Interpolation between cell values was carried out using the GOCAD interpolation method Discrete Smooth Interpolation (DSI), which is basically a linear interpolation method that considers the geometry of spatial (geologic) boundaries (Mallet, 1992). Linear interpolation is assumed to be adequate given the high density of data and the regular distribution of values.

2.4 Calibration: spoil cone-internal structuring

Reference data about internal bulk density distribution was collected from spoil cones at the Wolkenberg site in the direct neighbourhood of Chicken Creek in early 2008 (Maurer et al., 2008). Direct sampling on the catchment was not possible because invasive sampling methods would have implied a massive disturbance. Thus, two adjacent spoil cones that had, by eye, a comparable substrate composition. These spoil cones were dumped in November/December 2007 and were not bulldozed or artificially compacted in any other way.

HESSD
8, 4641–4699, 2011

Sampling was carried out by subsequently digging off three vertical cross sections through the spoil cones, each with a horizontal distance of 1 m, up to a maximal depth of 1.50 m. Each cross section profile was sampled using a specially designed cube-shaped shovel with a defined volume of 1 l (Fig. 12a). Samples were stored and transported in plastic bags. Sample points were arranged in a grid with a vertical spacing of 0.3 m and a horizontal spacing of 0.5 m. The total length of each cross section was 7 m. The coordinates (WGS84) of each cross section's extremities were recorded with a differential GPS (Trimble R8, Trimble Navigation Ltd., Sunnyvale).

For the determination of bulk-densities, overall 161 volume-samples were analyzed. Fresh mass was determined by weighting, samples were air dried and weighed again to determine volumetric water contents. Skeleton was removed after air drying and weighed separately for all samples. Additionally, particle size distributions of selected samples were determined using wet sieving for the sand fractions and the classic pipette method for the silt and clay fractions (Gee and Bauder, 1986).

The resulting point data were geo-referenced using the d-GPS coordinates and visualized in 3-D using GOCAD. A central compaction zone exists within each spoil cone, albeit not clearly defined (Fig. 12b, c). Bulk densities range from 1.3 to 1.6 g cm^{-3}. The data were used to calibrate the parameters ρ_{b0} and $\rho_{b,c}$. Heterogeneities in particle size distribution could not be detected within single spoil cones, which can mainly be ascribed to the applied sampling method..

3 Results and discussion

3.1 Construction of the spatial framework and uncertainties

The main requirement for the structure generator was the definition of the catchment borders. The 3-D-representation of the surface catchment has an area of 59 245 m^2, the subsurface catchment (i.e. the approximate surface of the clay base liner) has an

HESSD
8, 4641–4699, 2011

area of 60 898 m^2. Slight uncertainties exist about the surface of the clay base liner due to the fact that – for the most parts – only borehole data exist (Fig. 9a). Surface and subsurface catchment area do not exactly overlap, so the exact lateral delineation of the catchment is slightly uncertain, too (Fig. 9c, d). Connecting the surface and subsurface catchment borders to construct a lateral boundary surface seemed to be the most straightforward solution. Using this approach, the constructed 3-D-body of the entire catchment (lake area excluded) has a volume of 120 659 m^3 and contains 1208340 grid cells. Cell dimensions are 1 m × 1 m × 0.2 m (vertical).

Volume analysis (Table 5) indicates that the initially applied sediment masses (data from 19 October 2004) took up a 27 % larger volume than the sediment body after the terminal bulldozing. This finding can be ascribed to subsequent consolidation and compaction by bulldozers. If we assume initial mean bulk densities as were found at the comparable Wolkenberg site (1.45 g cm^{-3}), compaction would have resulted in an increased bulk density of about 1.84 g cm^{-3}. Presuming these bulk densities, the mass of the applied substrate was calculated to be in the magnitude of about 232 000 tons. The volume of the central trench was filled up during the bulldozing process. The volume discrepancy of about 40 000 m^3 between material removed from *s_0410* (42 000 m^3 from the west and 20 000 m^3 from the east part, totalling about 62 000 m^3) and the volume of the trench (about 22 000 m^3, Table 5) must also be explained by compaction: assuming that the trench filling has the calculated final bulk density (1.84 g cm^{-3}), about 51 000 m^3 of material with the original bulk density (1.45 g cm^{-3}) have been inserted in the trench, leaving about 11 000 m^3 volume surplus on both sides, which most probably was also lost due to compaction processes. Information on the intensity of compaction and the associated technical processes thus needs to be incorporated in the future.

Analysis of dumped ridge heights showed that maximal heights of dumped sediment account for almost 12 m above the clay base liner. One tier of spoil ridges was applied in the eastern part and two tiers of spoil ridges were applied in the western part. However, the analysis also suggests that the uppermost tier in the western part, i.e. more than 6 m of sediment, was completely displaced by bulldozing. The average height

HESSD
8, 4641–4699, 2011

difference for {*s_0410 – s_clay*} was calculated to be 2.56 m; however, this value does not necessarily reflect mean spoil ridge heights, as most areas have already been bulldozed. Results of {*s_0410 – s_0511*} suggest that an average of about 0.54 m was cut off from the initial ridges. Also, maximum values of {*s_0511-s_clay*} indicate heights of 3.5 m (east) and 3.7 m (west). These maximum values – on the other hand, are possibly also a result of the displacement of material from peripheral spoil ridges towards the centre. It must also be presumed that stacker dumping is configured to produce constant ridge heights. Thus, for the first model scenario, we assumed a constant spoil ridge height of 3 m.

3.2 Generated 3-D structures

Results of the process-based structure generator approach are shown exemplary for one realization of structural heterogeneity of the eastern half of the Chicken Creek catchment (Fig. 13), denoted as volume of interest in the following. The modelled volume of the sediment body has a surface extension of 18 568 m^2, almost 1.9 ha, which constitutes about a third of the area of the entire artificial catchment (see Sect. 2.1). Based on aerial image analysis, it was assumed that the whole volume was regularly filled with spoil ridges (Fig. 10a). The manually specified spatial location of the structural elements (spoil ridges) may fluctuate within narrow margins (1–2 m) because of subjective errors during digitization and the incomplete spatial information available. We expect though that these uncertainties have only a small impact on the overall results.

A sub-region containing the volume of interest was defined in the volume body. The limits were defined as the intersection line between surfaces *s_0410* and *s_clay* on the eastern side of the catchment. This sub-region has a volume of 43 918 m^3, containing 353476 cells with dimensions of 1 m × 1 m × 0.2 m.

Data were imported as aggregated values. For the present realization, a predefined (dimensionless) aggregation factor $D_A = 7$ was used. That means that 7 × 7 data

HESSD
8, 4641–4699, 2011

points were combined into one by calculating the arithmetic mean (see Sect. 2.4.3). One value thus covers an area of 49 cm^2 in a modelled spoil cone cross-section. The defined distance between cross-sections along the spoil ridges was 3 m, and a general continuous height of 3 m was appointed for spoil ridges. The total length of the stacker trajectory (i.e. the combined length of spoil ridges) simulated was 4254 m, which resulted in 1886 spoil cone cross sections along the trajectory. The total number of calculated data points representing the basic volume elements in the dataset thus accounted for 2927642. The dataset contained property values for bulk density and skeleton, coarse sand, medium sand, fine sand, silt and clay contents.

Due to the much lower resolution of the volume body's cell grid, the original values from the structure generation process were aggregated in the cells of the volume body (see above). After aggregation, 100242 cells actually contained values, thus representing about 44 % of the total cell number in the volume of interest (230587). Property values for the remaining cells were calculated in the following linear interpolation process using Direct Smooth Interpolation (DSI).

Upscaling and interpolation caused slight distortions of the value distribution and statistical parameters of the original dataset. As can be seen for the example of the fine sand content, upscaling and interpolation result in slight increases of mean and median values, whereas standard deviation and variance are reduced (Table 6). Likewise, the 25th and 75th percentiles are slightly moving towards the arithmetic mean. Value distribution shifts from rudimental bimodal towards unimodal normal distribution after interpolation (Fig. 14).

3.3 Particle size distributions and bulk density

Spatial patterns of generated structural heterogeneity are similar to those observed in reality (Fig. 13c, f). However, sediment distributions are a result of the rather simple substrate-mixing and pattern-imitating approach. The average particle size distribution (here for fine sand fraction) in the catchment model does not exactly resemble

HESSD
8, 4641–4699, 2011

the distribution that was measured on samples from the 20 m × 20 m grid (here for fine sand, Tables 2 and 6, Fig. 14 panel A1). However, the simulated distributions are representing the arithmetic means of particle size distributions of all geologic units that were used for substrate mixing (Tables 3 and 6). These effects were intentional, as our main goal was to reproduce heterogeneity patterns in a first step. We expect that a future process-based substrate mixing approach that considers the geologic conditions at the excavation site will generate model realizations that show more realistic particle distributions. However, the heterogeneity of quaternary sediment types at the excavation site in combination with the missing information about the exact origin of the parent material will still imply uncertainty.

The comparison between observed average bulk densities in non-compacted spoil cones and average bulk densities in the volume of interest (Table 7) indicated an overestimation of bulk density in the first realization of the spatial model. Here, mean values of 1.56 g cm^{-3} were calculated (respectively 1.53 g cm^{-3} in the dataset before interpolation), whereas the mean value from spoil cone sampling was 1.46 g cm^{-3}. Despite we already defined lower basic bulk density values for the impact zone (1.4 g cm^{-3}) as proposed by Matschak (1969), calculated values seem to be still too high. Overestimation of bulk densities was probably caused by incorrect choice of other relevant input parameters, e.g. stacker drop height (here $H_D = 5$ m).

An applicable method for conditioning spatial models with local hard data was proposed by Michael et al. (2010): they combined process-based geologic modelling with multiple-point geostatistical simulations using training images from object-based modelling. The results were geologically realistic spatial models that were fully conditioned to measurements. Similar combinations of a process-based structure generator and geostatistical data conditioning approaches have been presented elsewhere (e.g., Teles et al., 2004; Reza et al., 2006). Such comparisons with a well-characterized study site are imperative for the evaluation of hydrological models (de Marsily et al., 2005).

HESSD
8, 4641–4699, 2011

3.4 Mass balance

The total substrate mass contained in the volume of interest was calculated from the known cell sizes and bulk densities. In the spatial model, cells were arranged parallel to the SGrid top surface (i.e. ground level), which means that – if top and bottom surface are not parallel – smaller cell sizes occur along the bottom surface. This resulted in a slightly lower mean value of 0.191 m^3 for cell volumes instead of 0.2 m^3. Thus, each cell contained an average mass of 292.5 kg, resulting in a total mass of 67 445 tons for the volume of interest.

This value differs from the original mass input from the structure generator due to several reasons:

(a) The "volume" of the dataset – as it consists of individual "point" values – is not clearly defined. However, estimations in GOCAD gave a volume enclosed by an enveloping surface of 64 146 m^3.

(b) The fixed height of spoil cones, as derived from assumptions on stacker dumping technology and DEM analysis involves a larger enveloping volume of the original dataset. Regular spoil ridge heights cause the upper parts of cones located in zones with low distances between clay base liner and initial surface (i.e. zones with low values for *s_0511 – s_clay*) to protrude from the volume body's surface. Thus, the estimation of the enveloping volume rather corresponds with the volume *s_0411 – s_clay* (64 146 vs. 66 867 m^3).

This initially larger volume is intentional: in our model conception, the stacker is more likely to produce cones of continuously equal height, which were then lapped in the subsequent levelling process by bulldozers. The lapped material is subsequently provided as a filling for the central trench, hereby undergoing intense reworking and homogenization. Compaction resulting from the bulldozing process will further reduce volume and increase bulk density.

HESSD
8, 4641–4699, 2011

4 Conclusions

We present a structure generator capable of reproducing characteristic sediment heterogeneity patterns of an artificially constructed hydrologic catchment. The approach is based on information about technical processes at two spatial scales including dumping and particle segregation within individual spoil cones and the distribution of spoil cones along dumping trajectories. The structure generator creates distributed texture (skeleton; fine, medium, coarse sand; silt; clay) and bulk density data in relatively high resolution for the 2-D-vertical cross-sections and spatially aggregated for the 3-D catchment scale. The "scalability" of the model is useful when analyzing effects of sediment structures on flow processes with hydrological models. The 3-D structures and patterns can be used to investigate the effects of heterogeneity on different scale levels.

The results suggest that spoil cones with a compacted zone are forming characteristic spatial patterns typical for the technology. Particle segregation additionally modifies sediment properties. The effect of the patterns with respect to the distribution of soil hydraulic properties is obviously important for hydrological analyses. The stochastic mixing of parent materials produces structural heterogeneities that reproduce observed spatial patterns. The results indicate that a physically-based modelling of sediment structures is possible. The virtual catchment uncertainty can be easily considered by introducing stochastic components at each step of structure generation. The model can be further improved based on availability of data and each step can be calibrated separately. Up to now, the structure generator is only capable of reproducing characteristic sediment heterogeneity patterns resulting from stacker dumping. Results do not yet fully comply with the actually observed sediment distributions on "Chicken Creek". This will be achieved in the next steps by conditioning to measurement data and the comparison of geostatistic and deterministic approaches.

A future approach that simulates conditions on the excavation site is expected to produce more realistic sediment distributions. Also, the structure generator currently

HESSD
8, 4641–4699, 2011

reproduces only a part of the structural conditions on the artificial catchment test site. Subsequent processes of substrate scrapping, translocation and filling as well as compaction due to bulldozing need yet to be implemented to obtain a complete representation of the initial substrate distribution. In combination with the extensive monitoring of the Chicken Creek catchment, a thorough testing of spatial model scenarios and realizations will be possible. The results will help to model the catchment's hydrology, e.g. by deriving soil hydraulic properties via pedotransfer functions on different scale levels. The deterministic reproduction of the initial sediment distribution is also a precondition for the explanation of many aspects of ecosystem behaviour.

5 List of symbols

Name	Dimension	Key
*Csc*max	[–]	factor for spoil cone sediment variation
*Csc*lmax	[–]	factor for single layer sediment variation
Czone	[L]	extension of the compaction zone
D_A	[–]	data aggregation factor
ds_m	[L]	predefined layer thickness
du	[L]	distance unit for cross section alignment
dx_m	[L]	horizontal extension of layer m
dxr_m	[L]	$\sim dx_m$ on the right of the central axis
dz_m	[L]	vertical extension of layer m
H	[L]	vertical extension of cone cross section
H_D	[L]	sediment drop height
H_k	[L]	reference elevation level
H_{max}	[L]	vertical distance from H_k
L	[L]	horizontal extension of cone cross section
$P1_i$	[MM^{-1}]	mass fraction sediment 1
$P2_i$	[MM^{-1}]	mass fraction sediment 2

HESSD
8, 4641–4699, 2011

P_i	[MM^{-1}]	mass fraction spoil cone sequence
Psc_i	[MM^{-1}]	mass fraction single spoil cone
$Pscl_i$	[MM^{-1}]	mass fraction single layer
R	[L]	vertical distance to adjacent spoil ridge
Xcoord	[L]	longitudinal coordinate
Xcorel	[L]	relative horizontal grid coordinate
Xinit	[L]	x-coordinate of the initial impact point
Xorig	[L]	spoil cone origin on spoil ridge
Xstep	[L]	longitudinal step length
$\boldsymbol{XY}_{\text{diff}}$	[L]	vector to next cross section
$\boldsymbol{XY}_{\text{trans}}$	[–]	cross section alignment vector
Ycoord	[L]	latitudinal coordinate
Ystep	[L]	latitudinal step length
Zcorel	[L]	relative vertical grid coordinate
Zd	[L]	distance *H-Zinit*
Zinit	[L]	z-coordinate of the initial impact point
α	[°]	spoil cone slope angle
β	[°]	angle of the oblique central axis
ζ_i	[L^{-1}]	particle segregation factor
ρ_b	[ML^{-3}]	bulk density
ρ_{b0}	[ML^{-3}]	base bulk density
$\rho_{b,c}$	[ML^{-3}]	base bulk density in compaction zone
$\mathbf{R}$	[–]	Rotation matrix
Xdiff	[L]	distance betw. cross Sect. 1 and 2 along the longitude
X_{pos1}	[L]	geogr. position (longitude) of spoil cone cross Sect. 1
X_{pos2}	[L]	geogr. position (longitude) of spoil cone cross Sect. 2

HESSD
8, 4641–4699, 2011

Xtrans	[L]	vector component of $\boldsymbol{XY}_{\text{trans}}$ for the longitude
Ydiff	[L]	distance betw. cross Sects. 1 and 2 along the latitude
Y_{pos1}	[L]	geogr. position(latitude) of spoil cone cross Sect. 1
Y_{pos2}	[L]	geogr. position (latitude) of spoil cone cross Sect. 2
Ytrans	[L]	vector component of $\boldsymbol{XY}_{\text{trans}}$ for the latitude

Acknowledgements. This study is part of the Transregional Collaborative Research Centre 38 (SFB/TRR 38) which is financially supported by the Deutsche Forschungsgemeinschaft (DFG, Bonn) and the Brandenburg Ministry of Science, Research and Culture (MWFK, Potsdam). The authors also thank Vattenfall Europe Mining AG (VEM) for providing the research site.

The authors thank Rossen Nenov, Marin Dimitrov, Ralph Dominik, Thomas Seiffert and Norman Lochthofen (project Z1 of the SFB/TRR 38) for preparing and providing monitoring data from the raster soil sampling campaign and drone imagery. Thanks to Vattenfall Europe Mining for providing photogrammetric DEMs, aerial images and geological information. Thanks also go to Alexander Shumantov, Gunter Bormann and Helga Koeller for the substantial help in the field and in the laboratory. We thank Uwe Buczko (University of Rostock) for his advice in adapting the spoil cone generator to the stacker technology.

References

Barbour, S. L., Chapman, D., Qualizza, C., Kessler, S., Boese, C., Shurniak, R., Meiers, G., O'Khane, M., Hendry, J., and Wall, S.: Tracking the evolution of reclaimed landscapes through the use of instrumented watersheds – a brief history of the Syncrude Southwest 30 Overburden Reclamation Research Program. Proceedings of the Instrumented Watershed Symposium, Edmonton, Canada, 2004.

Benischke, R., Harum, T., Reszler, C., Saccon, P., Ortner, G., and Ruch, C.: Karst water drainage in the Kaisergebirge (Tyrol, Austria) – Catchment delineation combining hydrogeological investigations and isotope methods with hydrological modelling, Grundwasser, 15(1), 43–57, 2010.

Bosch, F. P. and Muller, I.: Improved karst exploration by VLF-EM-gradient survey: comparison with other geophysical methods, Near Surface Geophysics 3(4), 299–310, 2005.

Brutsaert, W.: Hydrology: An Introduction. Cambridge University Press, Cambridge, UK, 2005.

HESSD

8, 4641–4699, 2011

Buczko, U. and Gerke, H. H.: Estimating spatial distributions of hydraulic parameters for a two-scale structured heterogeneous lignitic mine soil, J. Hydrol., 312(1–4), 109–124, 2005a.
Buczko, U. and Gerke, H. H.: Modeling two-dimensional water flow and bromide transport in a heterogeneous lignitic mine soil, Vadose Zone Journal, 5(1), 14–26, 2005b.
Buczko, U., Gerke, H. H., and Hüttl, R. F.: Spatial distributions of lignite mine spoil properties for simulating 2-D variably saturated flow and transport, Ecol. Eng., 17(2–3), 103–114, 2001.
de Marsilly, G., Delay, F., Gonçalvès, J., Renard, P., Teles, V., and Violette, S.: Dealing with spatial heterogeneity, Hydrogeol. J., 13(1), 161–183, 2005.
Gascuel-Odoux, C., Weiler, M., and Molenat, J.: Effect of the spatial distribution of physical aquifer properties on modelled water table depth and stream discharge in a headwater catchment, Hydrol. Earth Syst. Sci., 14, 1179–1194, doi:10.5194/hess-14-1179-2010, 2010.
Gauthier, M. J., Camporese, M., Rivard, C., Paniconi, C., and Larocque, M.: A modeling study of heterogeneity and surface water-groundwater interactions in the Thomas Brook catchment, Annapolis Valley (Nova Scotia, Canada), Hydrol. Earth Syst. Sci., 13, 1583–1596, doi:10.5194/hess-13-1583-2009, 2009.
Gee, G. W. and Bauder, J. W.: Particle size analysis, in: Methods of Soil Analysis – Part 1: Physical and Mineralogical Methods, edited by: Klute, A., Soil Science Society of America Book Series 5, Madison, Wisconsin, USA, 1986.
Gerke, H. H.: Exploring preferential flow in forest-reclaimed lignitic mine soil, Adv. Geoecol., 38, 380–387, 2006.
Gerwin, W., Raab, T., Biemelt, D., Bens, O., and Hüttl, R. F.: The artificial water catchment "Chicken Creek" as an observatory for critical zone processes and structures, Hydrol. Earth Syst. Sci. Discuss., 6, 1769–1795, doi:10.5194/hessd-6-1769-2009, 2009a.
Gerwin, W., Schaaf, W., Biemelt, D., Elmer, M., Maurer, T., and Schneider, A.: The artificial catchment "Hühnerwasser" (Chicken Creek): construction and initial properties. Ecosystem Development Vol. 1, Scientific Publications of the Brandenburg University of Technology, 2011.
Gerwin, W., Schaaf, W., Biemelt, D., Fischer, A., Winter, S., and Hüttl, R. F.: The artificial catchment "Chicken Creek" (Lusatia, Germany) – A landscape laboratory for interdisciplinary studies of initial ecosystem development, Ecol. Eng., 35(12), 1786–1796, doi:10.1016/j.ecoleng.2009.09.003, 2009b.
Gross, L. J. and Small, M. J.: River and floodplain process simulation for subsurface characterization, Water Resour. Res., 34(9), 2365–2376, 1998.

HESSD
8, 4641–4699, 2011

Grunwald, S., Barak, P., McSweeney, K., and Lowery, B.: Soil landscape models at different scales portrayed in virtual modelling language, Soil Science, 165(8), 598–615, 2000.
Gu, W. and Freer, J.: Patterns of surface and subsurface runoff generation, IAHS Publication series, 229, 265–273, 1995.
Gutierrez-Jurado, H. A., Vivoni, E. R., Harrison, J. B. J., and Guan, H.: Ecohydrology of root zone water fluxes and soil development in complex semiarid rangelands, Hydrol. Process., 20(15), 3289–3316, 2006.
Hammond, M. and Han, D.: Issues of using digital maps for catchment delineation. Proceedings of the Institution of Civil Engineers – Water Management, 159(1), 45–51, 2006.
Hangen, E., Gerke, H. H., Schaaf, W., and Huettl, R. F.: Assessment of preferential flow processes in a forest-reclaimed lignitic mine soil by multicell sampling of drainage water and three tracers, J. Hydrol., 303(1–4), 16–37, 2005.
Hinschberger, F., Fourmont, A., Macaire, J. J., Brehert, J. G., Guerin, R., and Bakyono, J. P.: Contribution of geophysical surveys to the study of fine grained lacustrine sediments. Application to the Salieve marsh (Massif Central, France). Bulletin de la Societé Geologique de France, 177(6), 311–322, 2006.
Holländer, H. M., Blume, T., Bormann, H., Buytaert, W., Chirico, G. B., Exbrayat, J.-F., Gustafsson, D., Hölzel, H., Kraft, P., Stamm, C., Stoll, S., Blöschl, G., and Flühler, H.: Comparative predictions of discharge from an artificial catchment (Chicken Creek) using sparse data, Hydrol. Earth Syst. Sci., 13, 2069–2094, doi:10.5194/hess-13-2069-2009, 2009.
Hooper, R. P.: Applying the scientific method to small catchment studies: A review of the Panola Mountain experience, Hydrol. Process., 15(10): 2039–2050, 2001.
Hu, L. Y. and Chugunova, T.: Multiple-point geostatistics for modeling subsurface heterogeneity: A comprehensive review, Water Resour. Res., 44(11), W11413, doi:10.1029/2008WR006993, 2008.
Kendall, C., McDonnell, J. J., and Gu, W. Z.: A look inside "black box" hydrograph separation models: a study at the Hydrohill catchment, Hydrol. Process., 15(10), 1877–1902, 2001.
Kendzia, G., Reißmann, R., and Neumann, T.: Targeted development of wetland habitats for nature conservation fed by natural inflow in the post-mining landscape of Lusatia. World of Mining – Surface & Underground, 60(2), 88-95, 2008.
Knappe, S., Haferkorn, U., Mattusch, J., Meissner, R., Rupp, H., and Wennrich, R.: Water and solute balances in recultivated lignite mining dump soils – field data and lysimeter experiments, Water Air and Soil Pollution, 157(1–4), 85–105, 2004.

HESSD
8, 4641–4699, 2011

Koltermann, C. and Gorelick, S. M.: Heterogeneity in sedimentary deposits: A review of structure imitating, process-imitating and descriptive approaches, Water Resour. Res., 32, 2617–2658, 1996.
Le Borgne, F., Treuil, M., Joron, J. L., and Lepiller, M.: Natural and EDTA-complexed lanthanides used as a geochemical probe for aquifers: a case study of Orleans valley's alluvial and karstic aquifers, Bulletin de la Societé Geologique de France, 176(6), 513–529, 2005.
Leibiger, H.: Über die Gesetzmäßigkeiten der Bodenentmischung beim Verkippen von Mischböden in Braunkohletagebauen, Freiberger Forschungshefte, A309, 1–103, 1964.
Mallet, J. L.: Discrete Smooth Interpolation in geometric modelling. Computer-Aided Design, 24(4), 178–191, 1992.
Matschak, H.: Beiträge zur Strukturforschung an Tagebaukippen, Teil 1. Rohdichteverteilung in Abhängigkeit von der Fallhöhe und anderen Faktoren. Bergbautechnik, 19, 287–293, 1969.
Maurer, T., Gerke, H. H., Dusek, J., and Badorreck, A.: A 3D-structural model of a lignitic mine soil based on classification and interpolation of profile images. Eurosoil 2008 Proceedings, Vienna, Austria, 2008.
Maurer, T., Schneider, A., and Gerke, H. H.: Reconstruction of the topography of the clay base liner and delineation of the subterranean watershed of the Chicken Creek catchment, Technical Report, SFB/TRR 38, Cottbus, 2009 (in German).
Michael, H. A., Li, H., Boucher, A., Sun, T., Caers, J., and Gorelick, S. M.: Combining geologic-process models and geostatistics for conditional simulation of 3-D subsurface heterogeneity, Water Resour, Res., 46, W05527, doi:10.1029/2009WR008414, 2010.
Miller, J. K., Sun, T., Li, H., Stewart, J., Genty, C., Li, D., and Lyttle, C.: Direct modelling of reservoirs through forward process based models: Can we get there?, paper 12729 presented at the International Petroleum Technology Conference, Kuala Lumpur, 2008.
Moreton, D. J., Ashworth, P. J., and Best, J. L.: The physical scale modelling of braided alluvial architecture and estimation of subsurface permeability, Basin Research, 14(3), 265–285, 2002.
Mozley, P. S. and Davis, J. M.: Relationship between oriented calcite concretions and permeability correlation structure in an alluvial aquifer, Serra Ladrones Formation, New Mexico, J. Sediment. Res., 66(1), 11–16, 1996.
Nicolau, J.-M.: Ronoff generation and routing on artificial slopes in a Mediterranean-continental environment: the Teruel coalfield, Spain, Hydrol. Process., 16, 631–647, 2002.
Niemann-Delius, C., Stoll, R. D., Drebenstedt, C., and Müllensiefen, K.: Der Braunkohlentage-

HESSD
8, 4641–4699, 2011

bau, Bedeutung, Planung, Betrieb, Technik, Umwelt, Springer, Berlin, 2008.
O'Callaghan, J. F. and Mark, D. M.: The extraction of drainage networks from digital elevation data. Computer Vision Graphics and Image Processing, 28(3), 323–344, 1984.
Piotrowski, J. A., Geletneky, J., and Vater, R.: Soft-bedded subglacial meltwater channel from the Welzow-Sud open-cast lignite mine, Lower Lusatia, eastern Germany, Boreas, 28(3), 363–374, 1999.
Reza, Z. A., Pranter, J. M., and Weimer, P.: ModDRE: A program to model deepwater-reservoir elements using geomorphic and stratigraphic constraints, Comput. Geosci., 32, 1205–1220, 2006.
Robinson, D. A., Binley, A., Crook, N., Day-Lewis, F. D., Ferre, T. P. A., Grauch, V. J. S., Knight, R., Knoll, M., Lakshmi, V., Miller, R., Nyquist, J., Pellerin, L., Singha, K., and Slater, L.: Advancing process-based watershed hydrological research using near-surface geophysics: a vision for, and review of, electrical and magnetic geophysical methods, Hydrol. Process., 22(18), 3604–3635, 2008.
Schneider, A., Gerke, H. H., and Maurer, T.: Elevation models of the surface of the Chicken Creek catchment, Technical Report, SFB/TRR 38, Cottbus, 2009 (in German).
Schneider, A., Gerke, H. H., and Maurer, T.: 3D initial sediment distribution and quantification of mass balances of an artificially-created hydrological catchment based on DEMs from aerial photographs using GOCAD, Phys. Chem. Earth, 36(1–4), 87–100, 2011.
Sciuto, G. and Diekkrueger, B.: Influence of soil heterogeneity and spatial discretization on catchment water balance modelling, Vadose Zone Journal 9(14), 955–969, 2010.
Sech, R. P., Jackson, M. D., and Hampson, G. J.: Three-dimensional modelling of a shoreface-shelf parasequence reservoir analog: Part 1. Surface based modelling to capture high-resolution facies architecture, Am. Assoc. Petr. Geol. B., 93(9), 1155–1181, 2009.
Siemers, J. and Dreybrodt, W.: Early development of karst aquifers on percolation networks of fractures in limestone, Water Resour. Res., 34(3), 409–419, 1998.
Stumpp, C., Engelhardt, S., Hofmann, M., and Huwe, B.: Evaluation of pedotransfer functions for estimating soil hydraulic properties of prevalent soils in a catchment of the Bavarian Alps, European Journal of Forest Research, 128(6), 609–620, 2009.
Teles, V., Delay, F., and de Marsily, G.: Comparison of genesis and geostatistical methods for characterizing the heterogeneity of alluvial media: Groundwater flow and transport simulations, J. Hydrol., 294, 103–121, 2004.
Whittig, L. D. and Allardice, W. R.: X-ray diffraction techniques, in: Methods of Soil Analysis

HESSD
8, 4641–4699, 2011

– Part 1: Physical and Mineralogical Methods, edited by: Klute, A., Soil Science Society of America Book Series 5, Madison, Wisconsin, USA, 1986.
Zaplata, M., Fischer, A., Winter, S., Schaaf, W., and Veste, M.: Development of an initial ecosystem – II. Vegetation dynamics and soil pattern in an artificial water catchment in Lusatia, NE Germany, in: Book of Abstracts, 39th Annual Conference GfÖ, edited by: Holzheu S., and Thies, B., Bayreuther Forum Ökologie 115, Bayreuth, 124, 2009.
Zappa, G., Bersezio, R., Felletti, F., and Giudici, M.: Modelling heterogeneity of gravel-sand, braided stream, alluvial aquifers at the facies scale, J. Hydrol., 325(1–4), 134–153, 2006.

HESSD
8, 4641–4699, 2011

Table 1. Data used for deriving spatial boundaries and determining sediment properties in the structure generator model.

structure/property	datasets	date/period of recording	data source	methods of data acquisition/ processing
initial catchment surface	DEM Nov 2005	2005/10/24	Vattenfall Europe Mining AG	Photogrammetric analysis of aerial photographs[a]
surface of the clay base liner	DEM Oct 2004 DEM March 2005 DEM July 2005	2004/10/19 2005/03/05 2005/07/05	Vattenfall Europe Mining AG	Photogrammetric analysis of aerial photographs
	clay base liner borehole data	March 2008–June 2009	SFB/TRR 38 measurement campaign	Drilling cores and d-GPS determination of position
subsurface catchment	DEM clay base liner	based on measurement data, see above	SFB/TRR 38	SAGA GIS Deterministic 8 algorithm
volumes/masses dumped and relocated during construction	DEM Oct. 2004 DEM Nov 2005 DEM clay base liner	2004/10/19 2005/11/24	Vattenfall Europe Mining AG* SFB/TRR 38	Construction and calculation of volumes in GOCAD
spoil ridge position and configuration	aerial orthophoto	2004/10/19	Vattenfall Europe Mining AG	digitization in GOCAD
	orthophotomosaic	2009/09/10	SFB/TRR 38 drone based aerial suvey	
internal distribution of the solid phase campaign	particle size distribution drill core sampling,	October 2005–April 2006	SFB/TRR 38 measurement	20 m× 20 m and 40 m × 40 m borehole raster grid
	particle size distribution in selected spoil cones	January 2005		Soil sampling of eleven spoil cones during construction
original sediment properties at the excavation site	geological cross-sections along excavator steps	2004	Vattenfall Europe Mining AG	unknown
	particle size distributions	unknown		

[a] DEM from Nov 2005 was subsequently revised and enhanced, see Schneider et al. (2011).

HESSD
8, 4641–4699, 2011

Table 2. Texture data (fine earth fraction particle distributions of 220 soil samples) from raster soil sampling carried out in 2006, showing the differing values for the eastern and western part of the Chicken Creek catchment. Courtesy of subproject Z1, SFB/TRR 38.

	Coarse sand (630–2000 µm)	Medium sand (200–630 µm)	Fine sand (63–200 µm)	Sand fraction complete	Coarse silt (20–63 µm)	Medium silt (6.3–20 µm)	Fine silt (2–6.3 µm)	Silt fraction complete	Clay (<2 µm)
Eastern part	10.9	48.0	27.6	86.5	3.8	2.7	1.6	8.0	5.5
Western part	13.1	42.8	26.1	82.1	4.6	3.6	2.2	10.5	7.4
Average on catchment	12.2	45.0	26.7	84.0	4.2	3.2	2.0	9.4	6.6

HESSD
8, 4641–4699, 2011

Table 3. Properties of the principal types of parent material from the excavation site.

Facies	Geological abbreviation	Petro-graphy	Skeleton %	Sand %			Silt %			Clay %
				coarse	medium	fine	coarse	medium	fine	
Glacio-fluvial afterset sediments	qsD2-(WA)//gf	sand, gravel	13.7	6.3	50.0	25.0	5.0	0.0	0.0	0.0
Ground moraine	qsD2//Lg	marly till	0.3	7.7	22.0	29.0	25.0	1.5	1.5	13.0
Ground moraine	qsD2//Lg	sandy till	1.8	8.5	23.5	45.0	8.0	4.0	3.2	6.0
Gacio-limnic foreset sediments	qsD2//b(vs)	silts	0.0	0.5	1.5	13.0	54.0	1.5	1.5	28.0
Gacio-limnic foreset sediments	qsD2//b(vs)	banded sands, fine sands	0.4	5.4	15.0	52.0	19.0	3.2	2.0	3.0

HESSD
8, 4641–4699, 2011

Table 4. Input parameters used in the present model scenario.

Parameter	*Csc*max	*Csc*lmax	*Czone*	D_A	ds_m	H	H_D	α	β	ρ_{b0}
Value	0.2	0.05	0.5 m	7	0.1 m	3 m	5 m	35°	15°	1.2 g cm^{-3}

HESSD
8, 4641–4699, 2011

Table 5. Deposited and translocated sediment volumes during Chicken Creek construction as calculated in GOCAD.

	Volume difference in m^3		
	s_0511-s_clay (sediment body after construction)	*s_0410-s_clay* (sediment volume prior to bulldozing)	*s_0410-s_0511* (differences indicate translocated volumes)
East	–	66 867	−20 406
West	–	89 942	−41 518
Central trench	–	–	21 764
Total volume	126 140	159 992	−40 160
	Vertical distance in m		
Mean height difference	2.1	2.6	−0.6/1.4
Max. height difference	3.7	11.9	−3.5/6.3

HESSD
8, 4641–4699, 2011

Table 6. Statistical values for the property "fine sand content" (in %) after aggregation and interpolation in GOCAD. Also see Fig. 14a–c.

	Original structure generator values	After aggregation in cells	After linear DSI interpolation between cells
Number of samples	2 554 785	100 242	230 587
Mean	34.4	34.4	34.8
Standard deviation	13.0	12.8	12.0
Variance	169	163	144
25th percentile	24.6	24.8	26.0
Median	34.0	34.0	34.5
75th percentile	44.1	43.8	43.3

HESSD
8, 4641–4699, 2011

Table 7. Statistical values for particle size distributions (in %) and bulk density after DSI interpolation. Size intervals are given in µm. The volume of interest (eastern part of the catchment) contained 230587 cells.

	Skeleton (>2000)	Coarse sand (630–2000)	Medium sand (200–630)	Fine sand (63–200)	Silt (2–63)	Clay (<2)	Bulk density ($g\,cm^{-3}$)
Minimum	0.0	0.0	0.0	0.0	0.0	0.0	1.09
25th percentile	0.1	2.2	15.1	26.0	9.0	0.5	1.49
Median	0.93	6.2	22.3	34.5	21.2	5.4	1.56
75th percentile	4.1	11.48	31.1	43.3	32.6	14.3	1.59
Maximum	44.5	38.3	68.4	86.7	74.0	50.5	1.85
Mean	3.7	7.7	23.5	34.8	21.7	8.8	1.54
Std. deviation	6.2	6.6	11.9	12.0	15.0	9.6	0.1
Variance	38	43	140	144	225	92	0.01

HESSD
8, 4641–4699, 2011

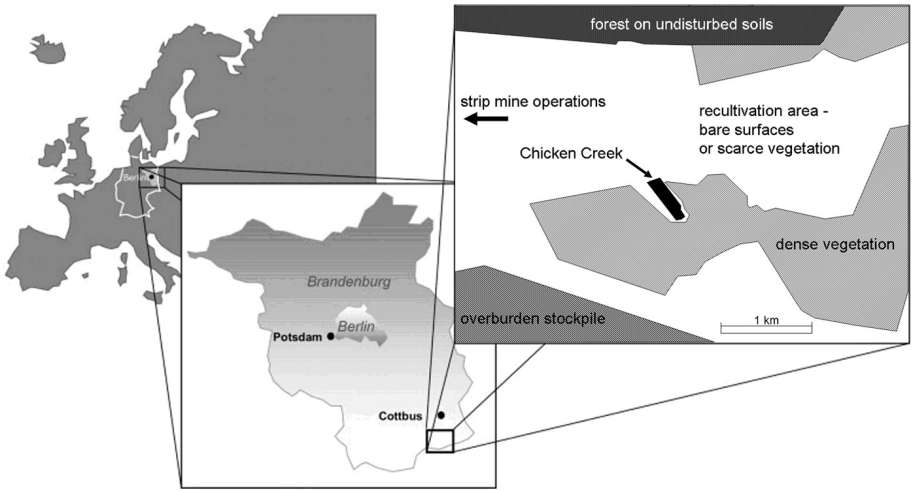

Fig. 1. Location of the artificial catchment.

HESSD
8, 4641–4699, 2011

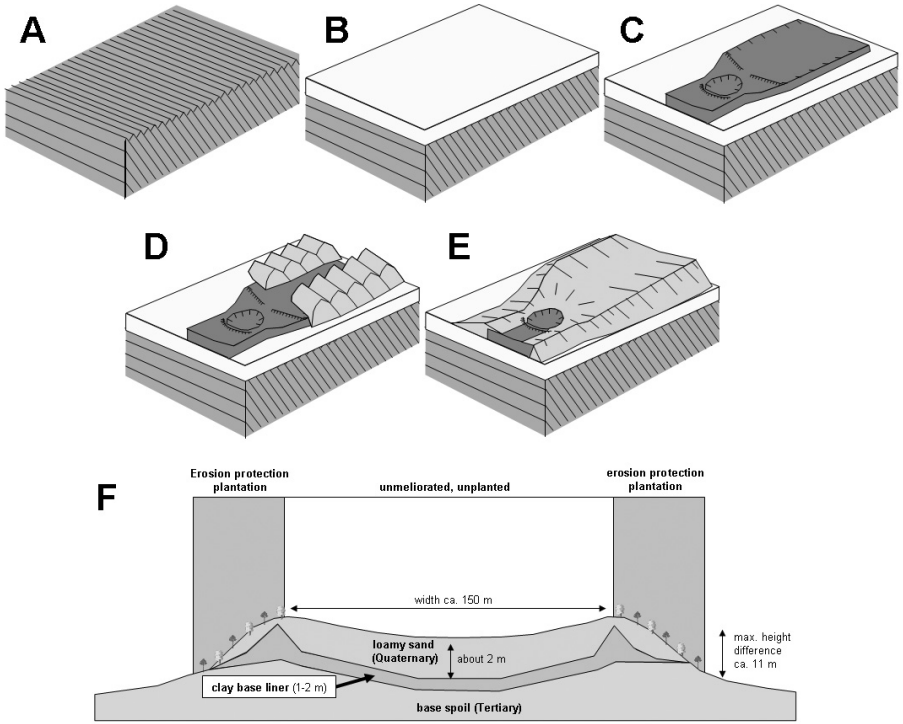

Fig. 2. Schematic overview of the "Chicken Creek" catchment construction steps **(A–E)** and schematic cross section **(F)**. Images courtesy by Werner Gerwin, BTU Cottbus (modified).

HESSD
8, 4641–4699, 2011

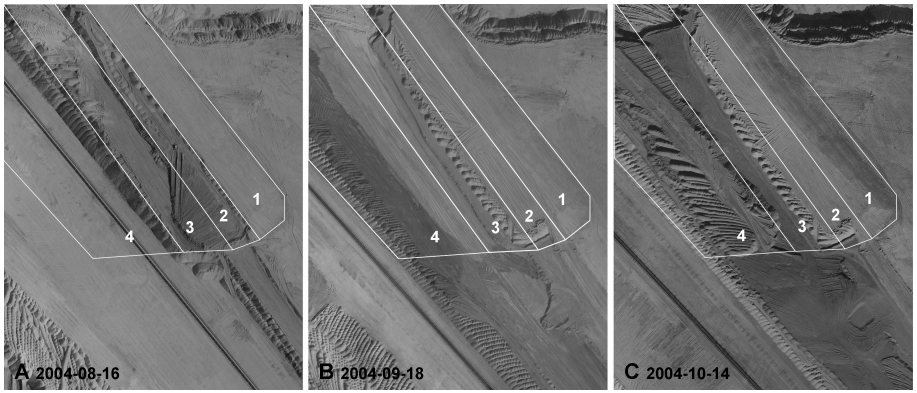

Fig. 3. Photographs of the construction phase, showing the progressive dumping of three bands, each consisting of the foundation layer of tertiary material, the ~1 m clay base liner and the cover layer of tertiary material.

HESSD
8, 4641–4699, 2011

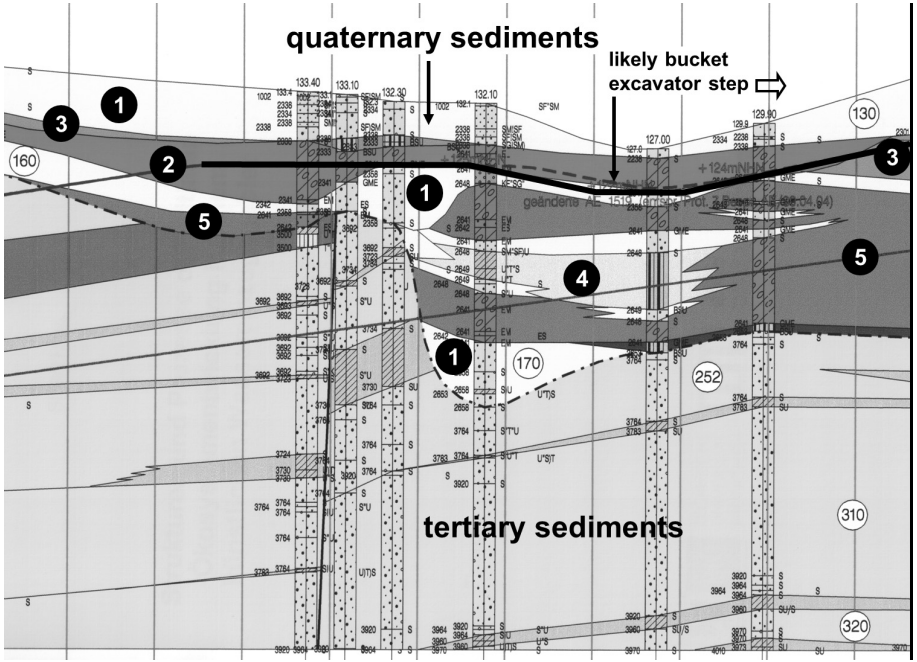

Fig. 4. Geological cross-section of the excavation site in 2004. The parent material was excavated during this time along the marked excavator route. Exact excavator positions during dumping were not recorded. (1) glacio-fluvial afterset sediments; (2) Drenthe-2 ground moraine; (3) upper Bänderschluff (varve); (4) relocated tertiary material; (5) Elster-2 ground moraine. Courtesy of Vattenfall Europe Mining AG.

HESSD
8, 4641–4699, 2011

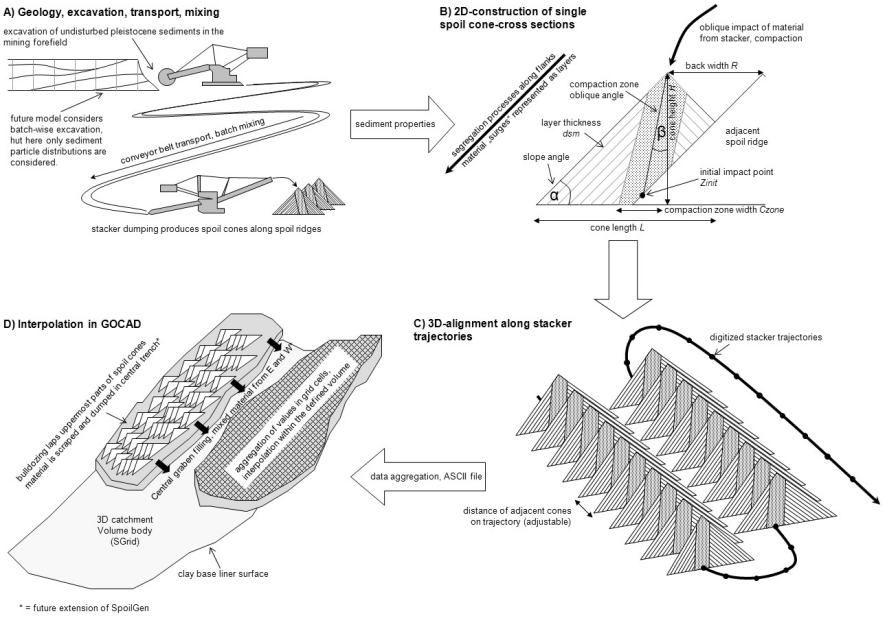

Fig. 5. Conceptual model: catchment construction steps.

HESSD
8, 4641–4699, 2011

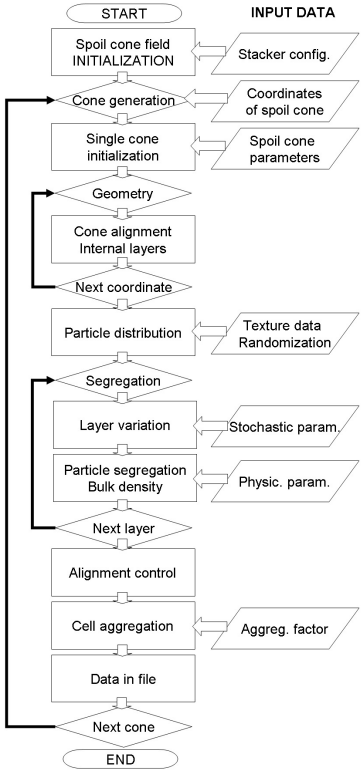

Fig. 6. Simplified flow chart diagram of the structure generator programme.

HESSD
8, 4641–4699, 2011

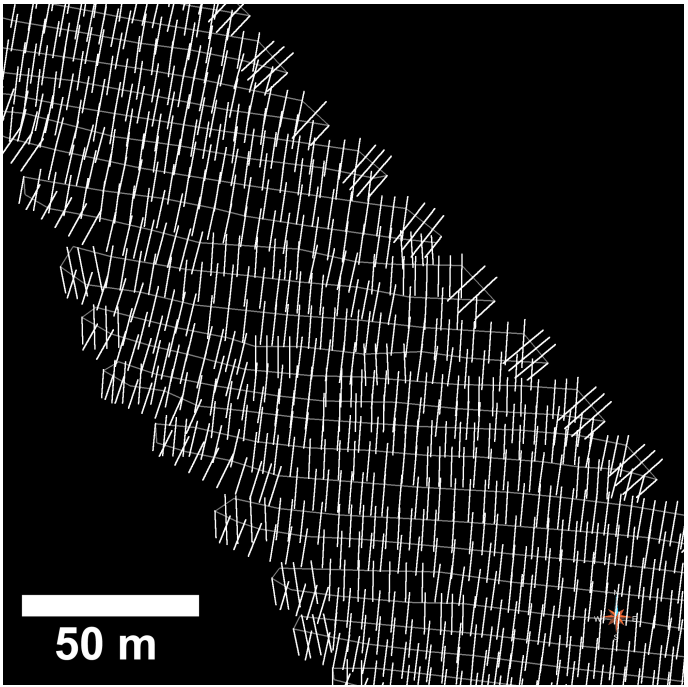

Fig. 7. The spatial alignment of 2-D cross sections (light grey) was derived from the spatial orientation of stacker trajectories (dark grey).

HESSD
8, 4641–4699, 2011

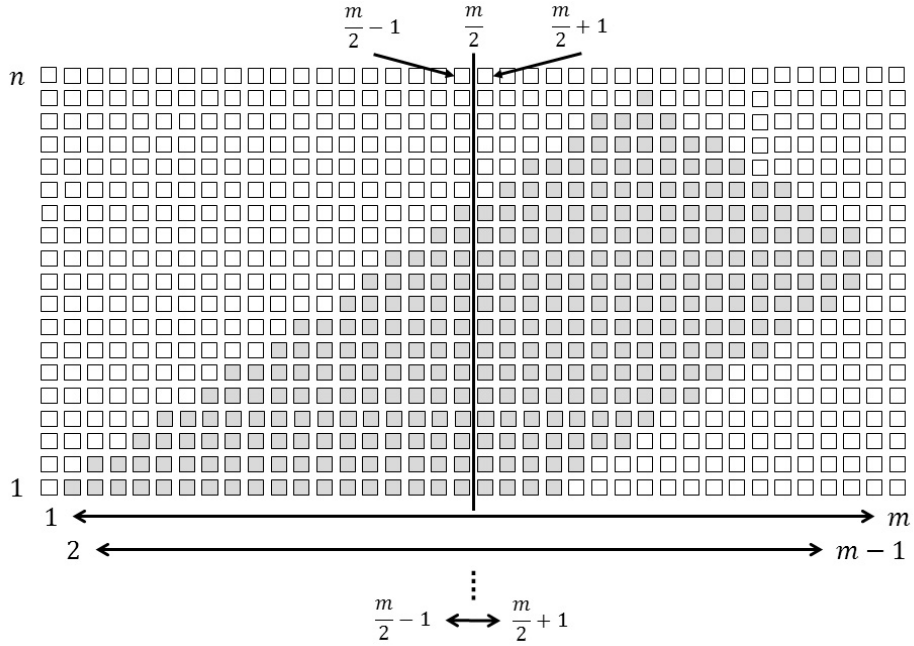

Fig. 8. Schematic demonstrating the principle of cross section flipping.

HESSD
8, 4641–4699, 2011

A structure generator for modelling initial sediment distributions

T. Maurer et al.

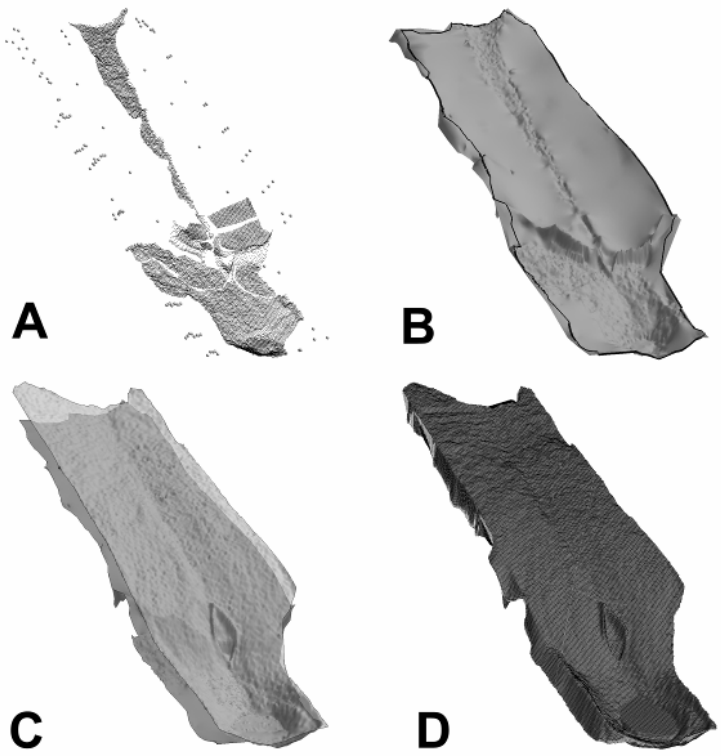

Fig. 9. (A) Point data (photogrammetry, boreholes as spheres) of the clay base liner; **(B)** clay base liner surface with subterranean catchment area; **(C)** clay base liner with the initial surface (November 2005), which was constructed from photogrammetric data; **(D)** resulting volume body (Stratigraphic Grid, SGrid).

HESSD
8, 4641–4699, 2011

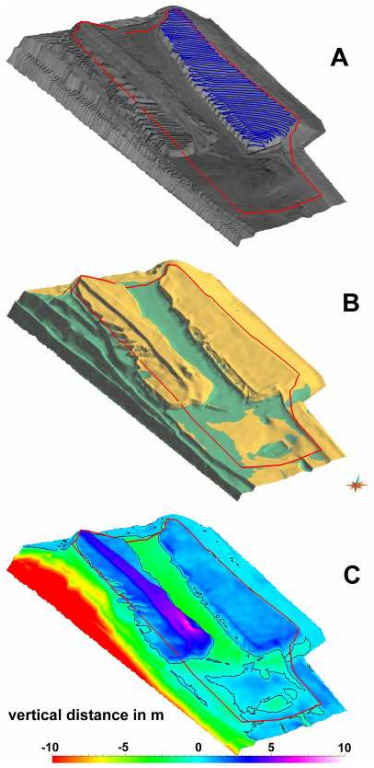

Fig. 10. The combination of aerial images with height information in GOCAD allowed the manual digitalization of spoil ridges **(A)**, the identification and calculation of volumes that were moved after stacker dumping **(B)** and to derive information about vertical distances and spoil cone heights **(C)**.

HESSD
8, 4641–4699, 2011

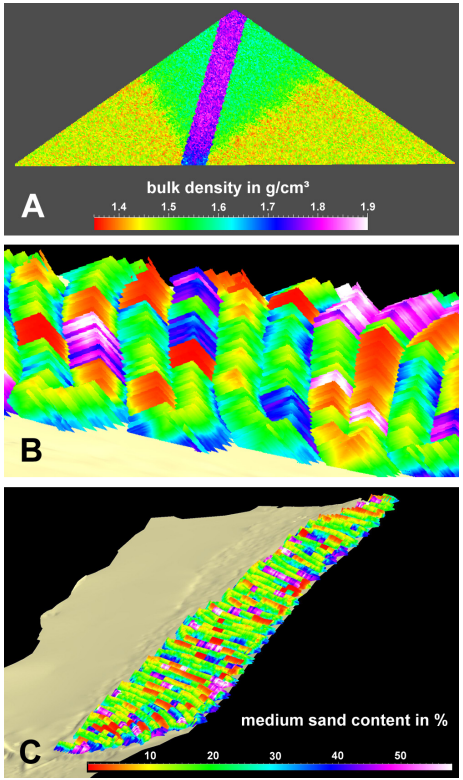

Fig. 11. Structure generator results shown as color-coded 3-D point data in GOCAD. **(A)** cross-section of a single spoil cone, featuring a compacted central zone; **(B)** side view of several spoil ridges, showing the lateral alignment of single cones; **(C)** a realization of spoil ridges on the complete eastern half of "Chicken Creek".

HESSD
8, 4641–4699, 2011

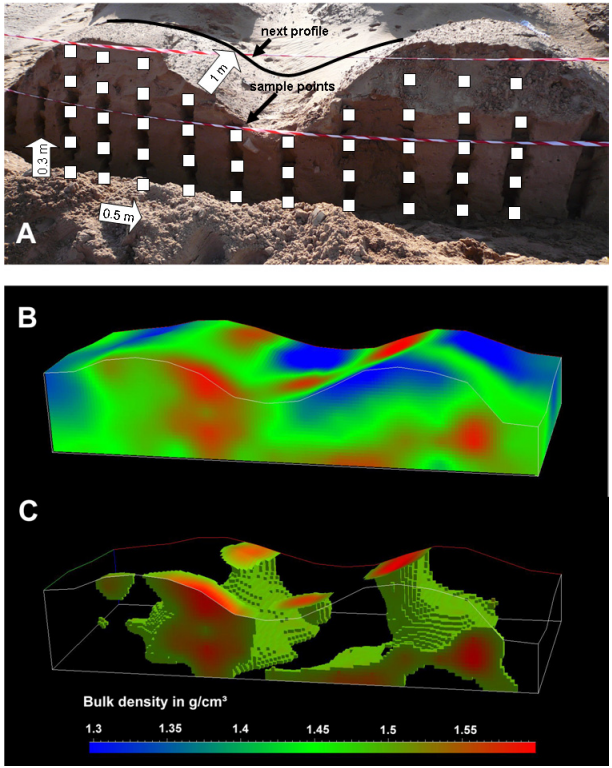

Fig. 12. 3-D-spoil cone sampling showing the spatial distribution of bulk densities: **(A)** Sampling of the spoil cones; **(B)** 3-D-Interpolation of bulk density in GOCAD; **(C)** showing only zones with highest densities (compaction).

HESSD
8, 4641–4699, 2011

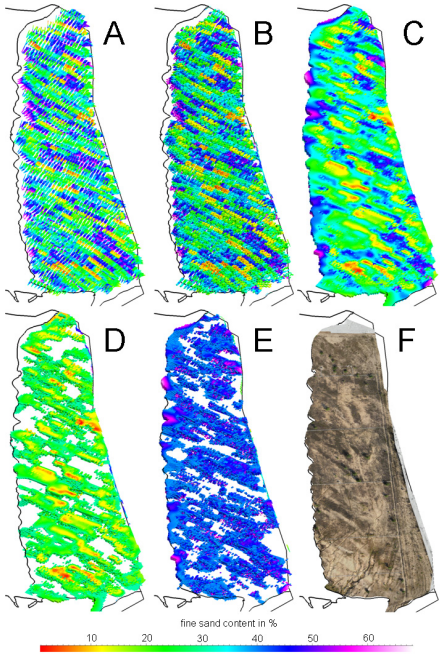

Fig. 13. GOCAD images depicting the 3-D spatial interpolation of data from the SpoilGen structure generator, exemplary given as fine sand contents on a realization of the eastern half of the Chicken Creek catchment: **(A)** individual values from the structure generator are imported in GOCAD; **(B)** Values are aggregated in the cells of the volume body. Cells containing no data are not shown. **(C)** Results of the 3-D linear interpolation (using DSI, Discrete Smooth Interpolation). **(D)** Areas containing only cells with 0–40 %, and **(E)** with 40–70 % fine sand content. **(F)** Aerial photograph showing heterogeneity patterns of the same region from September 2009.

HESSD
8, 4641–4699, 2011

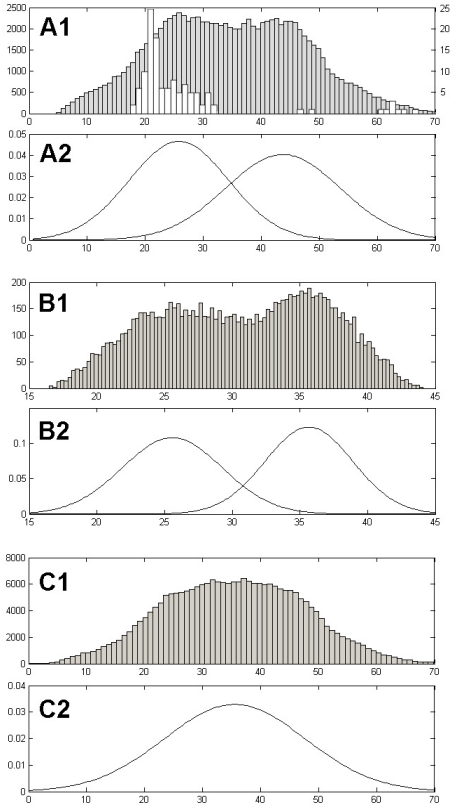

Fig. 14. Distribution of values (here: fine sand content) after aggregation of the original values (top) in the cells of the volume body (middle) and after linear interpolation (DSI) between the cells (bottom). The white bars in A1 show the histogram for measurement data from raster grid sampling.

HESSD
8, 4641–4699, 2011